Electrically pumped 1550 nm single mode III-V-on-silicon laser with resonant grating cavity mirrors

Yannick De Koninck,*[1,2] Gunther Roelkens[1,2] and Roel Baets[1,2]

[1] *Photonics Research Group, Department of Information Technology, Ghent University - imec*
[2] *Center for Nano-and Biophotonics (NB-photonics)*
Sint-Pietersnieuwstraat 41, B-9000 Ghent - Belgium
* *Corresponding author: yannick.dekoninck@intec.ugent.be*

Compiled October 22, 2014

An electrically pumped 1550 nm single mode III-V-on-silicon resonant mirror laser with record low threshold current is reported. The laser consists of 2 passive silicon grating cavities that both couple to the same III-V waveguide. Each silicon grating cavity behaves as a compact, narrow band reflector to the III-V waveguide such that a laser resonance arises inside the III-V waveguide. The resulting laser measures $160\mu m$ long and has a room-temperature threshold current of $4.1\,mA$. The laser is single mode with a side-mode suppression ratio of up to 48dB. © 2014 Optical Society of America

OCIS codes: 130.0250, 140.3948, 140.5960, 250.5960.

Over the past two decades, integrated photonics, and silicon photonics in particular, has gained importance as a technological enabler for a wide range of exciting new applications such as future high-speed short distance interconnects [1]. One of the key components in such densely integrated systems is the laser source. To bring laser functionality to the silicon platform, the most promising short-therm approach is the heterogeneous integration of III-V materials [2]. Ever since the first experimental demonstrations of this technology in the second half of the previous decade [3], there has been a trend to reduce the laser threshold and to lower the overall power consumption. Microdisk lasers [1] can reach sub-mA threshold currents but suffer from the absence of a strong wavelength selection mechanism which results in a low side-mode suppression ratio. Recent work on short-cavity DFB lasers shows that excellent continuous wave (CW), single mode laser performance can be accomplished with threshold currents as low as 8.8mA [4].

A novel approach, based on resonant mirrors and designed specifically for the III-V on silicon platform, was presented and studied extensively in [5]. Two identical passive silicon grating cavities are coupled to the same III-V waveguide above to form a linear device as shown schematically in figure 1a. Each silicon cavity is evanescently coupled to the InP waveguide. If the optical mode in the InP waveguide is of the silicon cavity's resonance wavelength, the silicon cavity will be excited. The energy built-up inside the silicon cavity couples back into the the InP waveguide both co- and counter-directionally to the incoming light. The co-directional light will interfere destructively with the InP waveguide mode while the counter-directionally coupled light propagates back into the III-V waveguide. Because CMOS manufacturing techniques allow for compact, high-Q silicon cavities, this approach enables high, narrow band reflectivity over a short distance. Moreover, resonant mirrors provide an elegant mechanism to couple the laser-generated light into

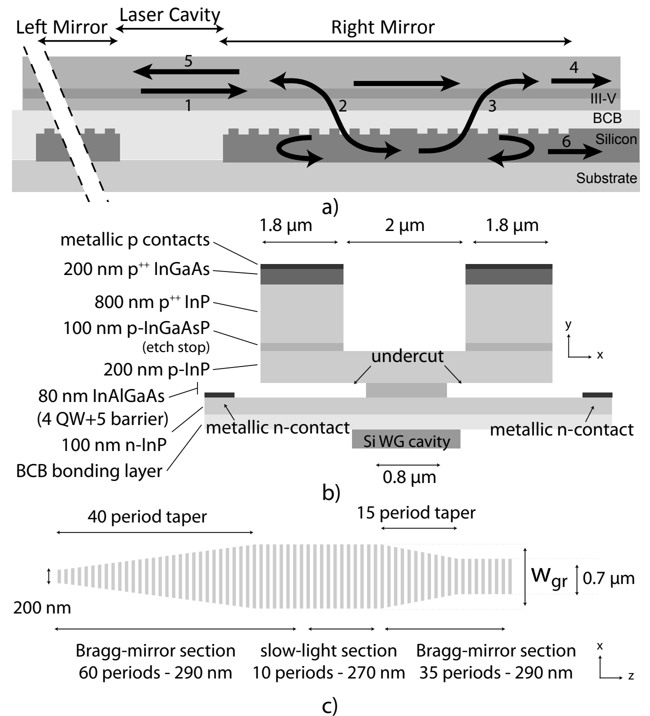

Fig. 1. top: schematic side-view of the operation of the resonant mirror laser. bottom: cross-section of the III-V mesa

an external silicon waveguide without the use of tapers: by coupling the silicon cavity to a silicon waveguide, a small fraction of the cavity mode leaks into that waveguide, which can be used as the laser output. An optically pumped proof-of-concept device [6] confirmed the potential advantages of using resonant mirrors as reflectors in III-V on silicon lasers. The threshold pump power of the experimentally demonstrated device was mW-level and the laser operated in single mode with a side-mode suppression ratio of up to 39dB. However, the practical us-

ability of optically pumped lasers is rather limited, since most applications require an electrical pumping mechanism. To achieve electrical pumping, metallic contacts have to be placed on the III-V waveguide structure to allow injection of electrical carriers. These metallic structures should be placed sufficiently far away from the optical mode to prevent excessive loss due to absorption in the metal and the highly doped (and absorbing) semiconductor used to make good ohmic contacts. This leads to a relatively thick III-V waveguide ($\sim 1-2\mu m$) with a typical effective index of ≈ 3.4. Moreover, such a large waveguide supports multiple transversal modes. In this work, laser sources are integrated on the widely adopted $220\,nm$ SOI platform. The effective index of a $220\,nm$ silicon slab waveguide is around $n_{eff,SOI} \approx 2.8$ at 1550 nm. In other words, when using the traditional approach to heterogeneous integration, the III-V laser mesa and the underlying SOI waveguide layer are far from phase-matched. As explained in [7], this phase mismatch deteriorates the operation of the resonant mirror because the silicon cavity leaks into the III-V mesa's higher order modes instead of into the desired fundamental mode. To overcome this problem, the effective index of the III-V waveguide should be reduced to better match the silicon cavity but still allowing a path for the electrical carriers to flow to the active region. It was proposed in [7] to do this by etching a wedge in the top layers to push the mode down and undercut the multi-quantum well (MQW) region to reduce the size and effective index of the III-V mode laterally. The proposed design is reproduced in figure 1b. A $2\,\mu m$ wide gap is etched in the top of the III-V mesa and the MQW are undercut to a width of $800\,nm$. By making these adjustments, the effective index of the III-V mode is reduced to $n_{eff,III-V} = 2.85$. Moreover, this III-V waveguide structure only supports a handful of higher order modes, all spaced sufficiently far away from the silicon cavity's resonance mode in both real and reciprocal space to prevent leakage from the cavity to these modes. Besides optical coupling efficiency between the III-V waveguide and the silicon cavity, the ability of the mirror to reflect light is also determined by the intrinsic Q-factor of the silicon cavity. In the optically pumped device, demonstrated in [6], the silicon cavity used was a 60 period shallow-etched grating with a quarter wave defect in the center. Due to scattering at the quarter-wave defect, the intrinsic Q-factor of this type of cavity saturates at around 4000, even for longer gratings. To reduce scattering at the defect, the quarter wave section was replaced by a 10 period ($275\,nm$ pitch) long slow-light section in between the $295\,nm$ period cavity mirror gratings, as shown in figure 1c. This improves the intrinsic Q-factor of an 80 period (total number of periods) grating by an order of magnitude from ~ 4000 to ~ 60000. Unwanted low-Q cavity modes exist near the facets of the grating. To prevent the III-V waveguide from coupling to these modes, the silicon grating is tapered to a narrower width away from the center. Figure 2 shows the reflection and transmission spectrum of the

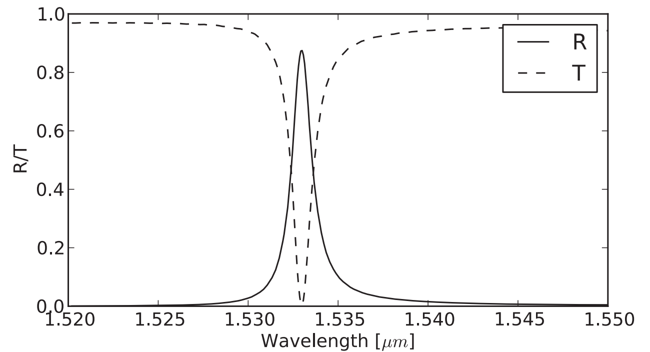

Fig. 2. Reflection and transmission of a resonant mirror with the optimized silicon grating cavity as shown in figure 1c

resonant mirror using the III-V waveguide cross-section shown in figure 1b and the silicon cavity illustrated in figure 1c, calculated using full-vectorial 3D FDTD [8]. The silicon grating is $1.5\,\mu m$ wide (w_{gr} and the distance between the bottom of the III-V layer and the top of the silicon layer is $200\,nm$. At its resonance wavelength, the mirror reflects 88% of the incoming light in a $1.27\,nm$ FWHM wavelength band. With a spacing of $100\,\mu m$ between the silicon cavities, the total length of the device adds up to $160\,\mu m$. Rate equation simulations show that in this case the threshold current lies between $1.5mA$ and $10\,mA$, depending on what value is considered for the Auger recombination rate and surface recombination rate. Another important metric in semiconductor lasers is the device's series resistance. Especially the p-doped slab connecting the pillars to the active region is of concern. The doping levels of the different p- and n-doped layers were designed as to trade-off low optical loss due to absorption and low series resistance. The total series resistance was estimated to be 37.4Ω. About half of this can be attributed to the p-doped slab connecting the pillar to the active region. The other half is evenly distributed between the pillar itself and the n-InP slab connecting the active region to the metallic n-contacts. Finally the thermal resistance between the active region and the silicon substrate was calculated using a commercial finite-element solver and yields 1.58K/mW. This high thermal resistance is mainly due to the thick $2\mu m$ SiOx buried oxide layer that prevents efficient heat flow from the laser to the underlying substrate.

To fabricate the III-V waveguide geometry depicted in figure 1 we developed a dedicated technological process. The patterned, passive SOI wafers fabricated in a multi-project wafer run with ePIXfab [9] and were fabricated in IMEC's 200mm CMOS pilot line. After thorough surface-clean and -preparation, a thin layer of Benzocyclobutene (BCB) [10] is spin coated on the SOI die and a 4mm by 8mm unpatterned InP die containing the appropriate epitaxial layers is bonded up-side-down on the SOI substrate. As shown on figure 1b, the III-V stack consists of a heavily p-doped InGaAs top contact layer on top of

an 800 nm thick p-doped InP layer making up the pillars. Underneath this heavily p-doped InP layer lies a 100 nm thick inGaAsP etch-stop layer to assure that the height of the lightly doped InP layer underneath, connecting the pillars to the active area, is always 200 nm. The 80 nm thick active layer consists of 4 strained InAlGaAs quantum wells enclosed by strain-compensating InAlGaAs barriers layers. The n-doped InP layer connecting the active area to the n-type metallic contacts is 100 nm thick. Before bonding, the III-V die is cleaned and a 150 nm SiOx layer is deposited to increase adhesion to the BCB and to set the distance between the bottom of the III-V stack and the top of the silicon waveguide to the desired value, since the BCB layer is around 40 nm. After BCB curing, the InP substrate and etch-stop layers are removed and what is left is a thin (approximately 1.5 μm thick) slab of III-V epitaxy. The pillars are defined in a SiO_2 hard mask using contact-lithography with manual alignment. The III-V layers are wet-etched in their appropriate acidic solutions (InP in HCl-based solutions and ternary/quaternary compounds in sulphuric or citric acid based solutions). After etching each layer of ternary or quaternary compound, a conformal silicon nitride film is deposited and immediately etched in a reactive ion etcher (RIE) using a highly anisotropic recipe. This technique covers the exposed side-walls of the etched ternary or quaternary compounds and prevents etching of these layers in future steps. Because the MQW region consists of quaternary InAlGaAs-based layers that will have to be etched (undercut) for a long time this sidewall protection is of major importance. Special attention should also be given to the mechanical stability of the InP structure. Immediately after undercutting the MQW region, the pillars are suspended and connected to the center part by the thin and fragile 200 nm thick p-doped InP layer. Although gravitational forces are of limited importance at such a small scale, fluidic forces, thermal expansion and internal stress can still render the structure mechanically unstable. For this reason the gap in between the pillars is reinforced with a 200 nm thick tensile strained silicon nitride layer. This increases the mechanical stability significantly and allows for safe etching of the MQW region. After the undercut is done, which takes around an hour in a stirred citric acid:H_2O_2 (20:1) bath, a thin layer of BCB is spin coated with the nitride reinforcement layer still in place. The diluted BCB solution will fill up the void created by the undercut and mechanically stabilise the structure. After the BCB is cured, all dielectric layers can be removed. The metallic n-contacts are deposited, the structure is planarized using a thick BCB layer, p-contacts are deposited, a via is etched to reach to the n-contacts underneath the BCB layer and finally thick gold-pads are deposited to facilitate electrical probing. Figure 3 shows a scanning-electron microscope (SEM) image of the device cross-section made using focused ion beam milling. The image shows the structure as proposed in the bottom panel of figure 1. The BCB layer is only 40 nm thick. Adding the 150 nm thick SiO_2

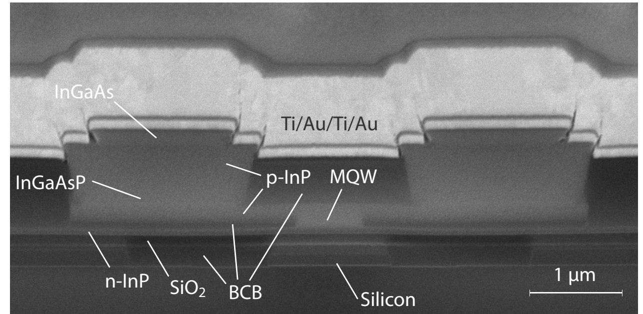

Fig. 3. SEM image of the device's cross-section showing the III-V mesa structure (including the MQW undercut) and the underlying silicon cavity.

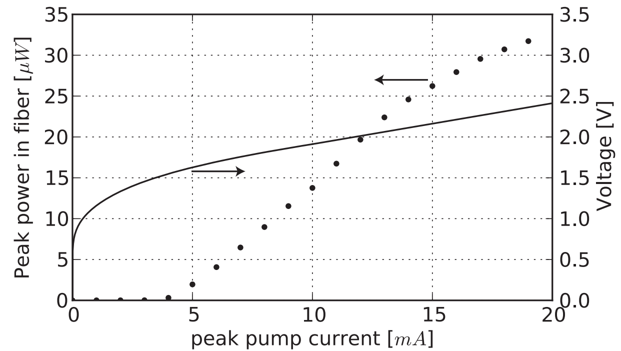

Fig. 4. Output power in the single mode fiber and voltage across the device measured at 20°C stage temperature as a function of current flowing through the junction, clearly showing the laser-threshold at 4mA

layer deposited on the InP die before bonding results in a total distance between the bottom of the n-InP layer and the top of the silicon waveguide of 190 nm. Each silicon cavity is 30μm long and the cavities are spaced 100 μm apart. Consequently the total device measures 160 μm in length. The devices were measured by connecting probe needles to the on-chip electrical pads and pumping them with 100 ns long current pulses with a pulse repetition interval of 5 μs. The laser couples the generated laser light into an SOI waveguide which leads to a grating coupler that diffracts the light into a single mode fiber. This fiber is directed into a 50/50 coupler sending half of the light into an optical power meter and the other half to an optical spectrum analyzer (OSA). Figure 4(left axis) shows the laser's LI curve plotting the laser's peak output power as a function of the peak current injected in the device at a stabilised stage temperature of 20°C. This image clearly shows the laser threshold at 4 mA. The optical output power shown on the graph is the measured peak output power coupled to single mode fiber. The fiber-coupler losses were measured to be 7dB and taking into consideration the fact that the laser emits on both sides (3dB), the total power emitted by the laser into the waveguide is about 10 times higher

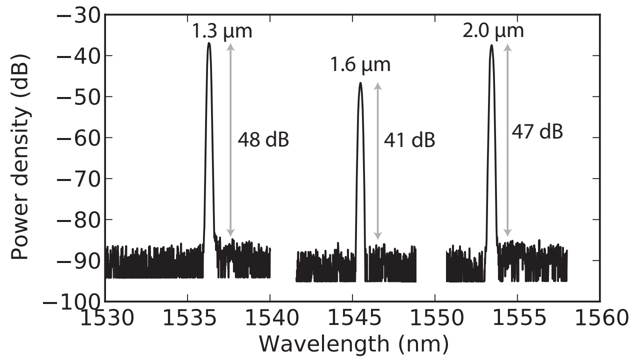

Fig. 5. Measured output spectrum of three quasi-identical lasers with different silicon cavity width: $1.3\mu m$, $1.6\mu m$ and $2.0\mu m$.

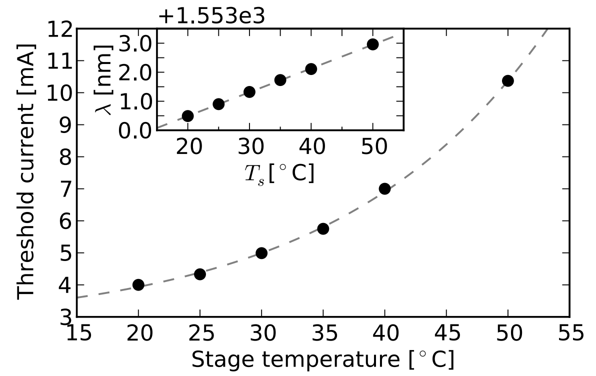

Fig. 6. Laser threshold and wavelength (inset) as a function of stage temperature.

than the values measured in the fiber and reported in figure 4. This yields a differential efficiency of approximately $30\mu W/mA$. The right axis of figure 4 shows the voltage across the device as a function of pumping current. Using this graph, the series resistance of the laser is measured to be $50\,\Omega$.

Figure 5 shows the spectra of 3 different lasers. These devices share the same III-V waveguide layout and length but differ in silicon cavity design: the width of the silicon grating cavity for these 3 lasers is $1.3\,\mu m$, $1.6\mu m$ and $2.0\,\mu m$ respectively. By adjusting the width of the silicon cavity waveguide, the effective index and consequently the resonance wavelength of the silicon cavity is altered. This measurement shows that the laser's operating wavelength is determined solely by the resonance wavelength of the silicon cavity. All three lasers operate in a single mode regime with a high side-mode suppression ratio of up to $48\,dB$. Continuous wave (CW) operation was not obtained. This is attributed to the high thermal resistance of the device measured to be 1.6K/mW. However, according to simulations, relatively simple measures such as adding a metallic heat spreader on top of the p-contact, can reduce the thermal resistance by a factor of 3, potentially paving the way to CW operation. The threshold (under pulsed operation) as a function of stage temperature is shown in figure 6 together with the laser emission wavelength (inset). In conclusion, we presented the first experimental demonstration of an electrically pumped hybrid silicon laser with resonant mirrors. The device measures $160\,\mu m$ in length and has a threshold current of 4mA. We showed that the lasing wavelength is determined by the resonance wavelength of the silicon cavities and that the narrow-band reflection spectrum of the resonant mirrors results in single-mode operation with a side-mode suppression ratio of up to 48dB.

The authors acknowledge partial support from IWT through the SBO-Glucosens project as well as from ERC through the InSpectra project. Yannick De Koninck thanks the research foundation Flanders (FWO) for a research grant.

References

1. T. Spuesens, J. Bauwelinck, P. Regreny, and D. Van Thourhout, "Realization of a Compact Optical Interconnect on Silicon by Heterogeneous Integration of IIIV," IEEE Photonics Technology Letters **25**, 1332–1335 (2013).
2. G. Roelkens, L. Liu, D. Liang, R. Jones, A. Fang, B. Koch, and J. Bowers, "III-V/silicon photonics for on-chip and inter-chip optical interconnects," Laser & Photonics Reviews **4**, 751–779 (2010).
3. A. W. Fang, H. Park, R. Jones, O. Cohen, M. J. Paniccia, and J. E. Bowers, "A continuous-wave hybrid AlGaInAs-silicon evanescent laser," IEEE Photonics Technology Letters **18**, 1143–1145 (2006).
4. C. Zhang, S. Srinivasan, Y. Tang, M. J. R. Heck, M. L. Davenport, and J. E. Bowers, "Low threshold and high speed short cavity distributed feedback hybrid silicon lasers," Optics Express **22**, 10202 (2014).
5. Y. De Koninck, G. Roelkens, and R. Baets, "Design of a Hybrid IIIV-on-Silicon Microlaser With Resonant Cavity Mirrors," IEEE Photonics Journal **5**, 2700413–2700413 (2013).
6. Y. De Koninck, F. Raineri, A. Bazin, R. Raj, G. Roelkens, and R. Baets, "Experimental demonstration of a hybrid III-V-on-silicon microlaser based on resonant grating cavity mirrors," Optics Letters **38**, 2496–2498 (2013).
7. Y. De Koninck, M. Tassaert, G. Roelkens, and R. Baets, "Design of an electrically-injected hybrid silicon laser with resonant mirrors," in "2013 IEEE Photonics Conference," (IEEE, 2013), pp. 327–328.
8. Lumerical Solutions http://www.lumerical.com, "Lumerical FDTD," .
9. The Silicon Photonics Platform-ePIXfab http://www.epixfab.eu, "ePIXfab," (2012).
10. S. Keyvaninia, M. Muneeb, S. Stanković, P. J. V. Veldhoven, D. V. Thourhout, and G. Roelkens, "Ultra-thin DVS-BCB adhesive bonding of III-V wafers , dies and multiple dies to a patterned silicon-on-insulator substrate," Optical Materials Express **3**, 1047–1056 (2013).